

# Anomalous dressing of Dirac fermions in the topological surface state of $\text{Bi}_2\text{Se}_3$ , $\text{Bi}_2\text{Te}_3$ , and $\text{Cu}_x\text{Bi}_2\text{Se}_3$

Takeshi Kondo, Y. Nakashima, Y. Ota, Y. Ishida, W. Malaeb, K. Okazaki, and S. Shin  
*ISSP, University of Tokyo, Kashiwa, Chiba 277-8581, Japan*

M. Kriener, Satoshi Sasaki, Kouji Segawa, and Yoichi Ando  
*Institute of Scientific and Industrial Research, Osaka University, Osaka 567-0047, Japan*  
 (Dated: December 11, 2013)

Quasiparticle dynamics on the topological surface state of  $\text{Bi}_2\text{Se}_3$ ,  $\text{Bi}_2\text{Te}_3$ , and superconducting  $\text{Cu}_x\text{Bi}_2\text{Se}_3$  are studied by 7 eV laser-based angle resolved photoemission spectroscopy. We find strong mode-couplings in the Dirac-cone surface states at energies of  $\sim 3$  and  $\sim 15\text{--}20$  meV, which leads to an exceptionally large coupling constant  $\lambda$  of  $\sim 3$ , which is one of the strongest ever reported for any material. This result is compatible with the recent observation of a strong Kohn anomaly in the surface phonon dispersion of  $\text{Bi}_2\text{Se}_3$ , but it appears that the theoretically proposed “spin-plasmon” excitations realized in helical metals are also playing an important role. Intriguingly, the  $\sim 3$  meV mode coupling is found to be enhanced in the superconducting state of  $\text{Cu}_x\text{Bi}_2\text{Se}_3$ .

PACS numbers: 79.60.-i, 73.20.-r, 72.15.Nj, 71.38.Cn

Topological insulators (TIs) are a new class of materials with Dirac fermions appearing on the surface [1]. The nature of Dirac fermions has already been actively studied in the graphitic materials [2], and it has been elucidated that the Dirac band dispersion is anomalously renormalized by such effects as electron-phonon interaction, electron-hole pair generation, and electron-plasmon coupling, leading to various intriguing properties [3–5]. While topological insulators are essentially understood within the noninteracting topological theory [6, 7], the Dirac fermions realized in real materials would be affected by nontrivial many body interactions, and hence the investigation of the quasiparticle dynamics is important for extending our understanding beyond the noninteracting regime. Since the Dirac fermions in TIs are distinct from those in graphitic materials in terms of their helical spin texture as well as possible interactions with a separate bulk electronic state, the low-energy excitations in the topological surface state are of particular interest. Indeed, such excitations are important not only for understanding many body interactions and couplings to other degrees of freedom in the topological surface state, but also for assessing the stability of putative Majorana fermions that are expected to emerge on the surface of superconducting TIs [8, 9].

In this context, there are already indications of the significance of many body interactions in the topological surface state. For example, a pronounced Kohn anomaly to indicate a strong electron-phonon coupling was recently observed in the surface phonon branch of  $\text{Bi}_2\text{Se}_3$  [10]; scanning tunneling spectroscopy (STS) uncovered an intriguing feature with finely-resolved sharp peaks at low energies ( $< 20$  meV) in the Landau-level spectra [11], pointing to an anomalous increase in the quasiparticle lifetime near the Fermi energy ( $E_F$ ). Theoretically, it has been proposed that a novel low-energy

collective mode called “spin-plasmon” would emerge as a consequence of the spin-momentum locking in the topological surface state [12]. Therefore, it is important to elucidate how the Dirac dispersion is renormalized close to  $E_F$ . However, so far the angle-resolved photoemission spectroscopy (ARPES) has not been able to detect any significant renormalization in the Dirac dispersions in TIs [13], possibly because of the lack of sufficient energy resolutions.

In this Letter, we demonstrate that the Dirac dispersion of the topological surface state is indeed anomalously renormalized, by using state-of-the-art ARPES with a 7-eV laser photon source. Availability of the ultra-high energy resolution ( $\sim 1$  meV) and the extremely low temperature ( $\sim 1$  K) [14] enabled us to detect low-energy kinks in the dispersion at  $\sim 3$  and  $\sim 15\text{--}20$  meV, giving evidence for hitherto-undetected mode couplings. The analysis of the kinks leads to the estimate of the coupling constant  $\lambda$  of as large as  $\sim 3$ , which is one of the largest reported for any material [15, 16]. Despite the existence of this boson-mode coupling, we observed no overall band reconstruction down to the lowest temperature, indicating that the topological surface state is protected from density-wave formations, which is usually expected to occur with such an extremely strong coupling with bosons [17–21].

Single crystals of  $\text{Bi}_2\text{Se}_3$  and  $\text{Bi}_2\text{Te}_3$  were grown by melting stoichiometric amounts of elemental shots in sealed evacuated quartz glass tubes. Superconducting samples of  $\text{Cu}_{0.24}\text{Bi}_2\text{Se}_3$  with  $T_c$  of 3.5 K and a shielding fraction of  $\sim 30\%$  [see Fig. 3(a)] were prepared by electrochemically intercalating Cu into the pristine  $\text{Bi}_2\text{Se}_3$  [22–25]. ARPES measurements were performed using a Scienta R4000 hemispherical analyzer with an ultraviolet laser ( $h\nu = 6.994$  eV) at the Institute for Solid State Physics (ISSP), University of Tokyo [26, 27].

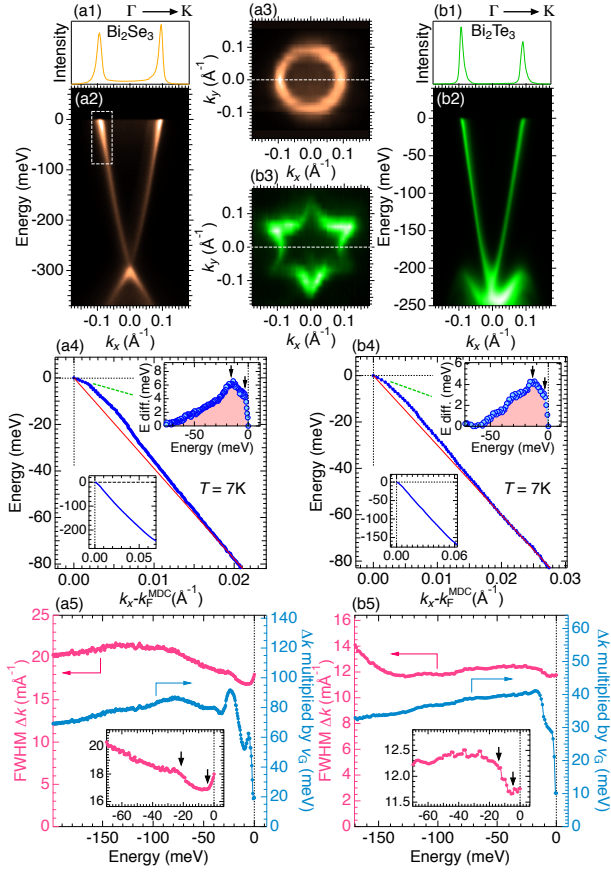


FIG. 1: (Color online) Data for (a1)-(a5) Bi<sub>2</sub>Se<sub>3</sub> and (b1)-(b5) Bi<sub>2</sub>Te<sub>3</sub>. (a1), (b1) MDC at  $E_F$ . (a2), (b2) Band dispersion map along  $\Gamma$ -K [dashed lines in (a3) and (b3)]. (a3), (b3) Fermi surface map. (a4), (b4) MDC-derived band dispersion. The same dispersion over a wide energy range is shown in the lower-left inset. The upper-right inset plots the energy difference from the linear dispersion. (a5), (b5) MDC peak width  $\Delta k$  (full width at half maximum, FWHM), and the  $\Delta k(E)$  multiplied by the group velocity  $v_G(E)$ . The inset shows the  $\Delta k(E)$  close to  $E_F$ .

Figures 1(a1)-(a5) and 1(b1)-(b5) show the ARPES data of Bi<sub>2</sub>Se<sub>3</sub> and Bi<sub>2</sub>Te<sub>3</sub>, respectively. The Dirac cones are clearly seen in the dispersion maps [Figs. 1(a2) and 1(b2)], and the shapes of the Fermi surface (FS) are very different between the two compounds [Figs. 1(a3) and 1(b3)]. In the present experiment, we did not observe any quantum-well states which emerge when adsorption of residual gases on the sample surface causes charge doping [28–34]. Also, our data are free from spectral intensity from the bulk conduction band, as can be clearly seen in Figs. 1(a1) and 1(b1) where the momentum distribution curves (MDCs) at  $E_F$  show only two sharp peaks from the Dirac dispersion.

The novel feature in our data is that the MDC-derived band dispersions [Figs. 1(a4) and 1(b4)] obviously deviate from straight lines, pointing to a large mass enhancement; the renormalized slope of the dispersion close to

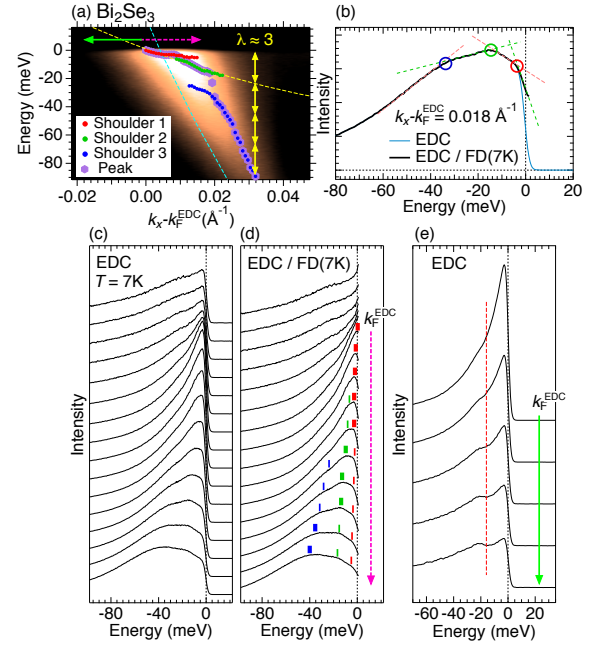


FIG. 2: (Color online) Data for Bi<sub>2</sub>Se<sub>3</sub> within a narrow range near  $E_F$  marked in Fig. 1(a2). (a) ARPES image; parabolic bands (dashed lines) with a mass of  $0.83m_e$  and  $0.14m_e$  [35] are superimposed. (b) Typical EDC with three features. (c) EDCs near  $k_F$  on the occupied-state side, and (d) those divided by Fermi function at  $T = 7$  K. Energies of shoulder-like structures [circles in (b) and bars in (d)] are plotted on (a). The energy eigenvalue for each  $k$ ,  $\varepsilon(k)$ , which is determined by the energy positions at which the spectral intensity becomes maximum, are indicated in (d) with bold bars, and plotted in (a) with thick filled hexagons. (e) EDCs beyond  $k_F$  (unoccupied-state side). The dashed line indicates the energy of the spectral dip.

$E_F$  is shown by dashed lines. As shown in the upper insets of Figs. 1(a4) and 1(b4), we calculate the energy difference between the putative linear dispersion (which is expected when the mode couplings are absent) and the measured one to estimate the strength of the coupling as a function of energy. We found anomalies at two energies,  $\sim -15$  and  $\sim -3$  meV, indicative of electron couplings with two different kinds of collective modes.

The effects of the couplings should also be observed in the energy dependence of the MDC peak width ( $\Delta k$ ) because of the Kramers-Kronig relation between  $\text{Re}\Sigma$  and  $\text{Im}\Sigma$  ( $\Sigma$  is the self-energy). In Figs. 1(a5) and 1(b5), we plot the obtained spectrum of  $\Delta k$  for Bi<sub>2</sub>Se<sub>3</sub> and Bi<sub>2</sub>Te<sub>3</sub>, respectively; as expected,  $\Delta k(E)$  presents kinks at the two energy scales,  $\sim -(15-20)$  and  $\sim -3$  meV, which are better seen in the insets. The  $\sim -3$  meV kink marks the onset of an anomalous increase in the magnitude of  $\Delta k(E)$  toward  $E_F$ .

To understand the complex behavior of the band dispersions revealed at low energy, we examine the shapes of the energy distribution curves (EDCs) around  $k_F$  shown

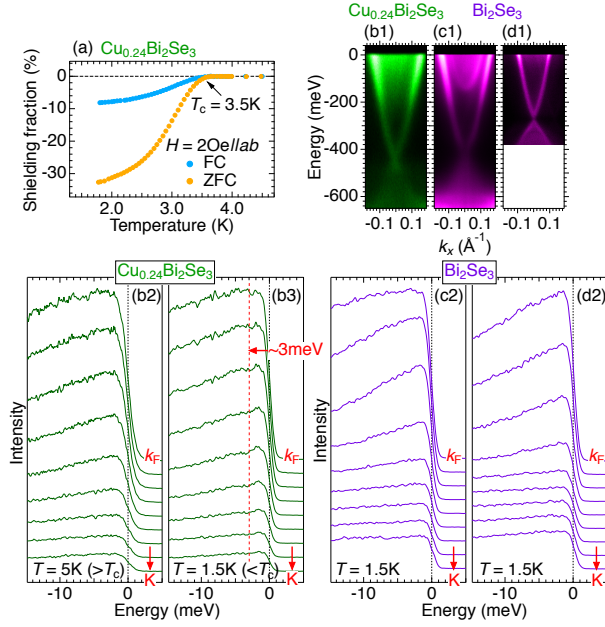


FIG. 3: (Color online) Data for  $\text{Cu}_{0.24}\text{Bi}_2\text{Se}_3$  superconductor with  $T_c = 3.5$  K and the pristine  $\text{Bi}_2\text{Se}_3$ . (a) Field-cooled (FC) and zero-field-cooled (ZFC) data of the superconducting shielding fraction of the sample used for ARPES experiments. Band dispersion map along  $\Gamma$ -K for (b1)  $\text{Cu}_{0.24}\text{Bi}_2\text{Se}_3$ , (c1) aged and (d1) fresh surfaces of  $\text{Bi}_2\text{Se}_3$ . EDCs of  $\text{Cu}_{0.24}\text{Bi}_2\text{Se}_3$  close to  $k_F$  measured (b2) above  $T_c$  and (b3) below  $T_c$ . The dashed line in (b3) indicates the spectral dip. EDCs of the pristine  $\text{Bi}_2\text{Se}_3$  close to  $k_F$  for (c2) aged and (d2) fresh surfaces.

in Fig. 2(c). In Fig. 2(d), those original EDCs are divided by the Fermi function at the measured temperature of 7 K convoluted with the experimental energy resolution, to remove the effect of Fermi cut-off. In the resulting curves, one can identify up to three shoulder-like features [an example for  $k_x - k_F^{\text{EDC}} = 0.018\text{\AA}^{-1}$  is shown in Fig. 2(b)], and the energy positions of those features are plotted on the ARPES image shown in Fig. 2(a). One can see in Fig. 2(d) that one of the shoulder-like features on the curves actually corresponds to the maximum; the dispersion of this maximum close to  $k_F$  is also plotted in Fig. 2(a) with thick filled symbols, and this dispersion is fitted with a parabolic dashed line in Fig. 2(a), giving a significantly enhanced effective mass of  $0.83m_e$  ( $m_e$  is the free-electron mass). For comparison, we also plot a putative band dispersion with a mass of  $0.14m_e$ , which was estimated for the bulk band from quantum oscillations [35]. The mass enhancement realized in the topological state is remarkable. Even more surprisingly, the estimated value of  $\lambda = v_0/v_F - 1$  ( $v_0$  and  $v_F$  are the bare-electron velocity [36] and the renormalized Fermi velocity, respectively) is as large as  $\sim 3$  as demonstrated in Fig. 2(a), which is one of the strongest coupling ever reported in any material [15, 16].

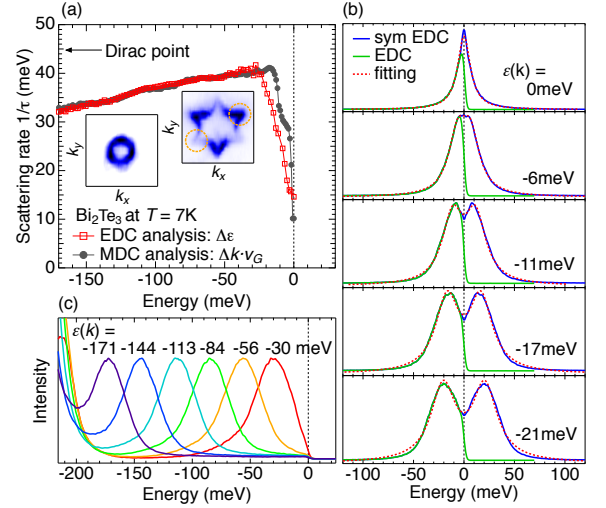


FIG. 4: (Color online) Results for  $\text{Bi}_2\text{Te}_3$ . (a) Scattering rate ( $1/\tau$ ) estimated from EDC peak width  $\Delta\epsilon$  (full width at half maximum, FWHM) as well as from the MDC peak width multiplied by the group velocity,  $\Delta k \cdot v_G$ . Insets show the ARPES map at  $-150$  meV (left) and  $E_F$  (right). (b) Estimation of  $\Delta\epsilon$  by fitting double Lorentzians to the symmetrized EDCs. (c) EDCs far from  $k_F$ ; the energy eigenvalue for each  $k$ ,  $\epsilon(k)$ , corresponds to the peak position in each EDC.

Perhaps the most direct way to demonstrate the strong mode-coupling is to present the peak-dip-hump structure in the EDCs. In Fig. 2(e), we show EDCs at  $k_F$  and beyond, where the peak-dip-hump shape is usually emphasized, and indeed, a clear dip can be seen at  $\sim -16$  meV (dashed line). However, a similar structure associated with the  $\sim 3$  meV mode is not clearly visible in the data of  $\text{Bi}_2\text{Se}_3$ .

Intriguingly, we found that a peak-dip-hump structure coming from the  $\sim 3$  meV mode coupling becomes visible in the superconducting samples of Cu-doped  $\text{Bi}_2\text{Se}_3$ . Figures 3(b2) and 3(b3) shows the EDCs of  $\text{Cu}_{0.24}\text{Bi}_2\text{Se}_3$  with  $T_c = 3.5$  K measured above and below  $T_c$ , respectively. The peak-dip-hump structure is seen at  $\sim 3$  meV below  $T_c$  but it is gone above  $T_c$ . We also measured the pristine  $\text{Bi}_2\text{Se}_3$  at the same condition ( $T = 1.5$  K), but did not observe the peak-dip-hump [Fig. 3(d2)]. Furthermore, we doped the surface of the pristine sample up to a doping level similar to that of  $\text{Cu}_{0.24}\text{Bi}_2\text{Se}_3$  by exposing it to residual gases [compare Figs. 3(c1) and (b1)], but again, the peak-dip-hump structure is not observed [Fig. 3(c2)]. Obviously, the enhancement of the  $\sim 3$  meV mode coupling has something to do with the superconductivity, and the origin of this enhancement needs to be scrutinized in future studies. In passing, we note that we did not detect any signature of the superconducting energy gap in the present experiment, probably because of the nonuniform surface condition after the sample cleaving. More elaborate studies would be required to nail down the topological superconductivity in  $\text{Cu}_x\text{Bi}_2\text{Se}_3$  [24] by

ARPES experiments.

Now we show the relevance of the mode couplings to the scattering rate ( $1/\tau$ ). Since the MDC width ( $\Delta k$ ) is not exactly the same as  $1/\tau$  for a curved band-dispersion, we have extracted the scattering rate with two methods: one simply uses the peak width of the EDCs ( $\Delta\varepsilon = 1/\tau$ ), the raw data of which are shown in Figs. 4(b) and 4(c); the other calculates the product of the MDC width and the experimentally obtained group velocity ( $\Delta k \cdot v_G \approx 1/\tau$ ). The behavior of  $\Delta k \cdot v_G$  in  $\text{Bi}_2\text{Se}_3$  and  $\text{Bi}_2\text{Te}_3$  are plotted in Figs. 1(a5) and 1(b5), respectively, which clearly reflect the mode couplings at  $\sim 20$  and  $\sim 3$  meV. Intriguingly, as shown in Fig. 4(a) for  $\text{Bi}_2\text{Te}_3$ , both  $\Delta\varepsilon$  and  $\Delta k \cdot v_G$  present a sharp reduction toward  $E_F$ . It is useful to note that this behavior is consistent with the STS result showing a sharpening of Landau-level peaks at low energies ( $< 20$  meV) [11].

One may also notice in Fig. 4(a) that  $1/\tau$  gradually decreases toward the Dirac point. This is unusual, because a monotonic *increase* in the electron-electron interaction with increasing binding energy is usually expected in conventional metals [37]. We speculate that this unusual behavior is a consequence of the fact that the penetration depth of the surface state increases as the momentum moves away from the Dirac point [38], which makes the surface state to gradually gain some bulk character. In fact, a feature to suggest such a variation is seen in the energy-contour maps plotted in the inset of Fig. 4(a): the contour near the Dirac point (left image) is almost circular, but close to  $E_F$  (right image), it exhibits a  $C_3$  modulation which reflects the symmetry of the bulk.

Now we discuss the most crucial question, namely, the origin of the bosons causing the anomalies at  $\sim -(15-20)$  and  $\sim -3$  meV in the ARPES spectra. A plausible candidate for the higher binding-energy one is the out-of-plane optical phonon mode  $A_{1g}^2$  with  $\omega = 21$  and 16 meV for  $\text{Bi}_2\text{Se}_3$  and  $\text{Bi}_2\text{Te}_3$ , respectively [39, 40]. It seems that  $\Delta k$  begins to decrease toward  $E_F$  [Figs. 1(a5) and 1(b5)] at almost the same energy as that of the  $A_{1g}^2$  mode. Also, the relevance of the phonon coupling is supported by the fact that the mode energy observed in  $\text{Bi}_2\text{Se}_3$  ( $\sim 20$  meV) is higher than that in  $\text{Bi}_2\text{Te}_3$  ( $\sim 15$  meV), which is consistent with the mass difference between Se and Te ( $\sqrt{m_{\text{Te}}/m_{\text{Se}}} = 1.27$ ).

As for the  $\sim 3$  meV mode, there are two possible origins. One is the optical mode of surface phonons. Recently, a strong Kohn anomaly was detected by a helium atom surface scattering (HASS) experiment in a phonon branch of  $\text{Bi}_2\text{Se}_3$  [10] at approximately  $2k_F^{\text{Dirac}}$  ( $k_F^{\text{Dirac}}$  is the Fermi momentum on the Dirac cone) with the characteristic energy of  $\sim 3$  meV, and this Kohn anomaly was attributed to the surface optical phonon mode [10]. However, Kohn anomaly is typically accompanied by an extensive FS nesting [20, 41, 42], which is absent in  $\text{Bi}_2\text{Se}_3$  [see Fig.1(a3)]. Also, the anomaly observed in the HASS experiment was isotropic [10], while the Kohn anomaly

is usually very anisotropic [20, 41, 42]. Hence, the Kohn anomaly in  $\text{Bi}_2\text{Se}_3$  is quite unusual. In our ARPES data, the  $\sim 3$  meV mode coupling in  $\text{Bi}_2\text{Te}_3$  is obviously weaker than that in  $\text{Bi}_2\text{Se}_3$ , even though in  $\text{Bi}_2\text{Te}_3$  the FS nesting on the Dirac cone is more pronounced [21] and hence the Kohn anomaly is expected to be stronger. In addition, the  $\lambda$  value of 0.43 has been obtained in the HASS experiment on  $\text{Bi}_2\text{Se}_3$  for the relevant phonons [43], but this value is obviously too small to account for the very strong coupling observed here for the  $\sim 3$  meV mode. Therefore, the surface optical phonons alone are obviously not sufficient for understanding the lower energy mode, and we need to seek for additional ingredients.

In this respect, another, more promising, origin of the  $\sim 3$  meV mode is the theoretically proposed “spin-plasmon”, which is suggested to have a maximum energy of  $\sim 2.2$  meV [12]. This mode consists of coupled plasmons and spin waves, and unlike the Kohn anomaly, it is expected for the round Fermi surface as in  $\text{Bi}_2\text{Se}_3$  [12]. The observed upturn in the MDC width toward  $E_F$  [see insets of Figs. 1(a5) and 1(b5)], which is not expected in a typical electron-phonon coupling, can be interpreted to signify an increasingly stronger interactions of the Dirac quasiparticles with spin-plasmons near  $E_F$ . Note that such strong interactions between the two are expected only when the plasmon spectrum does not overlap with the continuum of electron-hole excitations [3, 44], and hence the plasmon coupling should dominate the scatterings with  $q \sim 0$ . Therefore, it is natural that the quasiparticle scattering is enhanced toward  $E_F$  in this spin-plasmon scenario. All told, it is most likely that the large angle scattering ( $q \sim 2k_F$ ) by the surface optical phonons and the small angle scattering ( $q \ll 2k_F$ ) by the spin-plasmons both are playing roles in the enormously strong mass enhancement observed near  $E_F$  on the topological surface state.

In conclusion, we have investigated the quasiparticle dynamics in the topological surface state of  $\text{Bi}_2\text{Se}_3$ ,  $\text{Bi}_2\text{Te}_3$ , and  $\text{Cu}_x\text{Bi}_2\text{Se}_3$ . We found strong mode-couplings at the binding energy of  $\sim 15-20$  and  $\sim 3$  meV. The coupling to the  $A_{1g}^2$  phonons is proposed as the candidate for the former mode. As for the  $\sim 3$  meV mode, there are two possible origins. One is the optical mode of surface phonons. The other is the spin-plasmons, which are theoretically proposed as low-energy excitations of the helically spin-polarized Dirac fermions. Intriguingly, despite the extremely large mass enhancement factor  $\lambda$  of  $\sim 3$ , the topological surface state remains free from any band reconstruction down to the lowest temperature, indicating that the helical Dirac cone is protected from density-wave formations which are naturally expected for a system with extremely strong couplings to bosons.

This work is supported by JSPS (FIRST Program, NEXT Program, and KAKENHI 24740218), MEXT (Innovative Area “Topological Quantum Phenomena” KAKENHI 22103004), and AFOSR (AOARD 124038).

- 
- [1] M. Z. Hasan and C. L. Kane, Rev. Mod. Phys. **82**, 3045 (2010).
- [2] A. H. Castro Neto *et al.*, Rev. Mod. Phys. **81**, 109 (2009).
- [3] A. Bostwick *et al.*, Nature Phys. **3**, 36 (2007).
- [4] Y. Zhang *et al.*, Nature Phys. **4**, 627 (2008).
- [5] Y. Liu *et al.*, Phys. Rev. Lett. **105**, 136804 (2010).
- [6] L. Fu, C. L. Kane, and E. J. Mele, Phys. Rev. Lett. **98**, 106803 (2007).
- [7] J. E. Moore and L. Balents, Phys. Rev. B **75**, 121306(R) (2007).
- [8] L. Fu and C.L. Kane, Phys. Rev. Lett. **100**, 096407 (2008).
- [9] X. -L. Qi, T. L. Hughes, S. Raghu, and S. -C. Zhang, Phys. Rev. Lett. **102**, 187001 (2009).
- [10] X. Zhu *et al.*, Phys. Rev. Lett. **107**, 186102 (2011).
- [11] T. Hanaguri, K. Igarashi, M. Kawamura, H. Takagi, and T. Sasagawa, Phys. Rev. B **82**, 081305(R) (2010).
- [12] S. Raghu, S. B. Chung, X. -L. Qi, and S. -C. Zhang, Phys. Rev. Lett. **104**, 116401 (2010).
- [13] Z.-H. Pan *et al.*, Phys. Rev. Lett. **108**, 187001 (2012).
- [14] K. Okazaki *et al.*, Science **337**, 1314 (2012).
- [15] W. L. McMillan, Phys. Rev. **167**, 331 (1968).
- [16] P. Hofmann, I. Y. Sklyadneva, E. D. L. Rienks and E. V. Chulkov, New J. Phys. **11**, 125005 (2009).
- [17] K. Nasu, Phys. Rev. B **44**, 7625 (1991).
- [18] C. R. Ast and H. Höchst, Phys. Rev. Lett. **90**, 016403 (2003).
- [19] Y. M. Koroteev *et al.*, Phys. Rev. Lett. **93**, 046403 (2004).
- [20] E. W. Plummer *et al.*, Prog. Surf. Sci. **74**, 251 (2003).
- [21] Liang Fu, Phys. Rev. Lett. **103**, 266801 (2009).
- [22] M. Kriener *et al.*, Phys. Rev. B **84**, 054513 (2011).
- [23] M. Kriener, K. Segawa, Z. Ren, S. Sasaki, and Y. Ando, Phys. Rev. Lett. **106**, 127004 (2011).
- [24] S. Sasaki *et al.*, Phys. Rev. Lett. **107**, 217001 (2011).
- [25] M. Kriener, K. Segawa, S. Sasaki, and Y. Ando, Phys. Rev. B **86**, 180505(R) (2012).
- [26] T. Kiss *et al.*, Phys. Rev. Lett. **94**, 057001 (2005).
- [27] T. Kiss *et al.*, Rev. Sci. Instrum. **79**, 023106 (2008).
- [28] P. D. C. King *et al.*, Phys. Rev. Lett. **107**, 096802 (2011).
- [29] M. Bianchi, R. C. Hatch, J. Mi, B. B. Iversen, and P. Hofmann, Phys. Rev. Lett. **107**, 086802 (2011).
- [30] Z.-H. Zhu *et al.*, Phys. Rev. Lett. **107**, 186405 (2011).
- [31] H. M. Benia, C. Lin, K. Kern, and C. R. Ast, Phys. Rev. Lett. **107**, 177602 (2011).
- [32] L. A. Wray *et al.*, Nature Phys. **7**, 32 (2011).
- [33] M. Bianchi *et al.*, Nature Commun. **1**, 128 (2010).
- [34] S. R. Park *et al.*, Phys. Rev. B **81**, 041405(R) (2010).
- [35] K. Eto, Z. Ren, A. A. Taskin, K. Segawa, and Y. Ando, Phys. Rev. B **81**, 195309 (2010).
- [36]  $v_0$  was estimated from the slope of the putative linear dispersion in the absence of mode-couplings, shown as solid straight lines in Figs. 1(a4) and 1(b4).
- [37] T. Valla, A. V. Fedorov, P. D. Johnson, and S. L. Hulbert, Phys. Rev. Lett. **83**, 2085 (1999).
- [38] W. Zhang, R. Yu, H.-J. Zhang, X. Dai, and Z. Fang, New J. Phys. **12**, 065013 (2010).
- [39] W. Richter, H. Kohler, and C. R. Becker, Phys. Status Solidi B **84**, 619 (1977).
- [40] K. M. F. Shahil, M. Z. Hossain, D. Teweldebrhan, and A. A. Balandin, Appl. Phys. Lett. **96**, 153103 (2010).
- [41] E. Hulpke and J. Lüdecke, Phys. Rev. Lett. **68**, 2846 (1992).
- [42] E. Rotenberg, J. Schaefer, and S. D. Kevan, Phys. Rev. Lett. **84**, 2925 (2000).
- [43] X. Zhu *et al.*, Phys. Rev. Lett. **108**, 185501 (2012).
- [44] P. Hawrylak, Phys. Rev. Lett. **59**, 485 (1987).